International Journal of Heat and Mass Transfer 55 (2012) 6808–6818

Contents lists available at SciVerse ScienceDirect

International Journal of Heat and Mass Transfer

journal homepage: www.elsevier.com/locate/ijhmt

Numerical investigation of several physical and geometric parameters in the natural convection into trapezoidal cavities

Adriano da Silva [a,*], Éliton Fontana [b], Viviana Cocco Mariani [c,d], Francisco Marcondes [e]

[a] Escola de Química e Alimentos – Universidade Federal do Rio Grande – FURG Rua Barão do Caí, 125, 95500-000 Santo Antônio da Patrulha – RS, Brazil
[b] Departamento de Engenharia Química, Universidade Federal de Santa Catarina – UFSC, Brazil
[c] Departamento de Engenharia Mecânica, Pontifícia Universidade Católica do Paraná – PUCPR Rua Imaculada Conceição, 1155, Prado Velho, 81611-970 Curitiba, PR, Brazil
[d] Departamento de Engenharia Elétrica, Universidade Federal do Paraná – UFPR, Brazil
[e] Departamento de Engenharia Metalúrgica e de Materiais, Universidade Federal do Ceará – UFC Caixa Postal 12144, Fortaleza, CE, Brazil

ARTICLE INFO

Article history:
Received 28 September 2011
Received in revised form 25 June 2012
Accepted 25 June 2012
Available online 23 July 2012

Keywords:
Natural convection
Trapezoidal cavities
Baffles
Title angle
EbFVM

ABSTRACT

Natural convection in trapezoidal cavities, especially those with two internal baffles in conjunction with an insulated floor, inclined top surface, and isothermal left-heated and isothermal right-cooled vertical walls, has been investigated numerically using the Element based Finite Volume Method (EbFVM). In numerical simulations, the effect of three inclination angles of the upper surface as well as the effect of the Rayleigh number (Ra), the Prandtl number (Pr), and the baffle's height (H_b) on the stream functions, temperature profiles, and local and average Nusselt numbers has been investigated. A parametric study was performed for a wide range of Ra numbers ($10^3 \leqslant Ra \leqslant 10^6$) H_b heights ($H_b = H^*/3$, $2H^*/3$, and H^*), Pr numbers ($Pr = 0.7$, 10 and 130), and top angle (θ) ranges from 10 to 20. A correlation for the average Nusselt number in terms of Pr and Ra numbers, and the inclination of the upper surface of the cavity is proposed for each baffle height investigated.

1. Introduction

Natural convection in rectangular and non-rectangular cavities is a widely studied heat transfer phenomenon, because of its various engineering and industrial applications such as electronic equipment cooling, heat loss from solar collectors, food processing and storage, building insulation, electrochemistry, fire control, metallurgy, meteorology, geophysics, and flow in nuclear reactors. Many researchers have experimentally, analytically, and numerically investigated natural convection heat transfer in enclosures in recent decades.

Iyican et al. [1,2] first studied the problem of natural convection heat transfer in a closed trapezoidal cavity, presenting both analytical and experimental results. Their cavity was comprised of a cylindrical cold top, parallel to a hot horizontal surface and plane adiabatic side walls. Lam et al. [3] reported similar results for a trapezoidal cavity comprising of two vertical, adiabatic walls, a hot floor, and an inclined cold top wall. Lee [4] performed experiments in a nonrectangular cavity considering several Rayleigh (Ra) and Prandtl (Pr) numbers and various wall angles for aspect ratios equal to 3 and 6. Results indicate that the heat transfer and fluid motion within the enclosure are strong functions of the Ra number, the Pr number, and the orientation angle of the enclosure. Peric [5] presented results for the same problem investigated by Lee [4], but they differ both qualitatively and quantitatively from those shown by Lee [4]. Kuyper and Hoogendoorn [6] investigated how the inclination angle of isothermal walls (from 45° to 0°) influences the flow, and how the Ra number influences the average Nusselt number for laminar natural convection flow in trapezoidal cavities.

Natural convection in trapezoidal cavities in conjunction with internal baffles attached to the walls also has been investigated. Internal baffles have a significant effect on flow and heat transfer. Note that internal baffles take place in several technologies, typically in electronic equipment subject to cooling and heating and air movement around furniture. Following this line, Moukalled and Acharya [7–9] observed natural convection heat transfer in a trapezoidal cavity with partial dividers attached to either the lower horizontal base [7], the upper inclined surface of the cavity [8], or to both surfaces [9].

Moukalled and Darwish [10] studied natural convection in a partitioned trapezoidal cavity with one baffle attached to the lower horizontal base. They found that heat transfer decreases by increasing the Pr number and height of the baffle. Boussaid et al. [11] investigated heat transfer within a trapezoidal cavity, without baffles, heated at the bottom and cooled at the inclined top. Moukalled and Darwish [12] investigated the natural convection

* Corresponding author.
E-mail addresses: adrianosilva@furg.br (A. da Silva).

0017-9310/$ - see front matter © 2012 Elsevier Ltd. All rights reserved.
http://dx.doi.org/10.1016/j.ijheatmasstransfer.2012.06.088

Nomenclature

b	baffle	Re	Reynolds number
g	gravity acceleration, (m/s^2)	T	temperature, (K)
H	height of trapezoidal cavity, (m)	T_0	reference temperature, (K)
H^*	height of the cavity where the baffle is located, (m)	T_H	hot temperature, (K)
H_b	baffle height, (m)	T_C	cold temperature, (K)
i	interface	u	velocity in x direction, (m/s)
k_r	ratio between the thermal conductivity of the baffle and the fluid	v	velocity in y direction, (m/s)
L	length of trapezoidal cavity, (m)	W_b	baffle thickness, (m)
L_b	baffle locations, (m)	x, y	Cartesian coordinates, (m)
$\hat{n}$	unit vector normal to the baffle-fluid interface	α	thermal diffusivity, (m^2/s)
$\overline{Nu}$	average Nusselt number	β	thermal expansion coefficient of air, (1/K)
Nu_y	local Nusselt number	θ	inclination of the top wall of the cavity, (°)
p	pressure (Pa)	ν	kinematic viscosity, (m^2/s)
Pr	Prandtl number	ρ	fluid density, (kg/m^3)
Ra	Rayleigh number	$\vec{\nabla}$	gradient vector

in trapezoidal cavities with the baffle attached to the upper inclined surface. In addition, Moukalled and Darwish [13] researched the natural convection in trapezoidal cavities with two offset baffles, where one baffle was attached to the upper inclined surface and the other one was attached to the lower horizontal base. Natarajan et al. [14,15] studied natural-convection flow in a trapezoidal cavity (without baffles) with a uniformly heated bottom walls and linearly heated/cooled vertical walls. The average Nusselt number versus Ra number illustrates that the overall heat transfer rate at the bottom wall is larger for the linearly heated left wall and cooled right wall. Natural convection in trapezoidal cavities with the same boundary conditions used in [14,15] was investigated by Basak et al. [16] for various tilt angles of the side walls.

Tanmay et al. [17] investigated the natural convection within a trapezoidal cavity for uniformly and non-uniformly heated bottom walls, insulated top walls, and isothermal side walls with an inclination angle. They found that the average heat transfer rate does not vary significantly for the non-uniform heating of bottom walls. The steady natural convection of air flow in a trapezoidal room with inclined left heated wall (seven values), a vertical right cooled wall, and two insulated horizontal upper and lower walls were investigated numerically by Lasfer et al. [18]. Furthermore, Fontana et al. [19] studied the flow and heat transfer in trapezoidal cavities with two baffles placed on the horizontal surface. The effect of the height of the baffles and Pr number in the natural convection was investigated.

Tmartnhad et al. [20] studied mixed convection ($10 \leqslant Re \leqslant 1000$) from a trapezoidal cavity with a tilted wall of 22° where the inlet opening was horizontal or vertical, while the outlet was placed horizontally on the bottom wall. The results showed that the flow and heat transfer depends on the inlet opening. Moreover, the natural convection heat and mass transfer in an asymmetric trapezoidal cavity was studied in Papanicolaou and Belessiotis [21] for large values of the Ra numbers, $10^7 \leqslant Ra \leqslant 10^{10}$ where turbulent conditions prevail. Correlations for the mean convective heat and mass transfer coefficients were obtained. Paramane and Sharma [22] investigated the natural convection into trapezoidal and triangular cavities in order to performance an investigation of high order interpolation schemes. More recently, Roslan et al. [23] investigated the natural convection in trapezoidal cavities, where the effect of thermal conductivity and viscosity of the fluid were taken into account.

We investigate the effect of the angle of the top wall on the flow dynamics and heat transfer in a trapezoidal cavity, where two baffles are placed on the cavity's horizontal surface. While the numerical analyses of natural convection heat transfer in trapezoidal cavities related to this subject have been investigated [7–10,12,13,19], the inclination variation of the top wall has not. In previous research, the angle of the top wall (θ) of the cavity has only been equal to a certain angle (e.g., 15°); whereas, this paper takes into account three different angles (θ = 10°, 15°, and 20°). Thus, to the best of our knowledge, the effect of the inclination of the top wall on the natural convection in trapezoidal cavities has not yet been studied. We analyze in detail how the number and height (H_b) of adiabatic baffles (of finite thickness, $W_b = L/20$), and the ratio between the thermal conductivity of baffle and fluid ($k_r = 2$) affect heat transfer. It is important to mention that k_r equal to two corresponds to an intermediate value of a material like wood or plaster and all the investigated fluids. We consider $Pr = 0.7$ (air), $Pr = 10$ (water), and $Pr = 130$ (oil) as the working fluid in the range of Ra numbers ($10^3 \leqslant Ra \leqslant 10^6$). The top inclined wall and the horizontal surface are insulated, while the left and right vertical walls are kept isothermic at a higher and lower temperature, respectively. The EbFVM was employed to solve the nonlinear, coupled, partial differential equations for fluid flow and temperature fields. The results are shown in terms of isotherms, streamlines, and local and average Nusselt numbers. Correlations for the average Nusselt in terms of Pr numbers, Ra numbers, and the inclination of the upper surface of the cavity are presented for each baffle height investigated.

2. Mathematical formulation

The general schematic configurations of the two-dimensional trapezoidal cavities with two inside baffles are shown in Fig. 1a, along with the coordinates. Fig. 1b shows the grid refinement distributions employed for all numerical simulations. The vertical left and right walls of the trapezoidal cavity are heated and cooled, respectively, at constant temperatures T_H and T_C, where $T_H > T_C$. The horizontal surface and the inclined wall remain adiabatic. The width of the cavity (L) is four times the height (H) of the shortest vertical wall. Three inclinations of the upper wall of the cavity are investigated (10°, 15°, and 20°). Baffles are also placed at three heights ($H_b = H^*/3$, $2H^*/3$, and H^*) where H^* denotes the height of the cavity where the baffle is located. The baffle thickness, $W_b = L/20$, and baffle locations $L_{b1} = L/3$ and $L_{b2} = 2L/3$ are considered.

We assume the fluid properties to be constant. The exception is the density in the buoyancy force term in the y direction of the

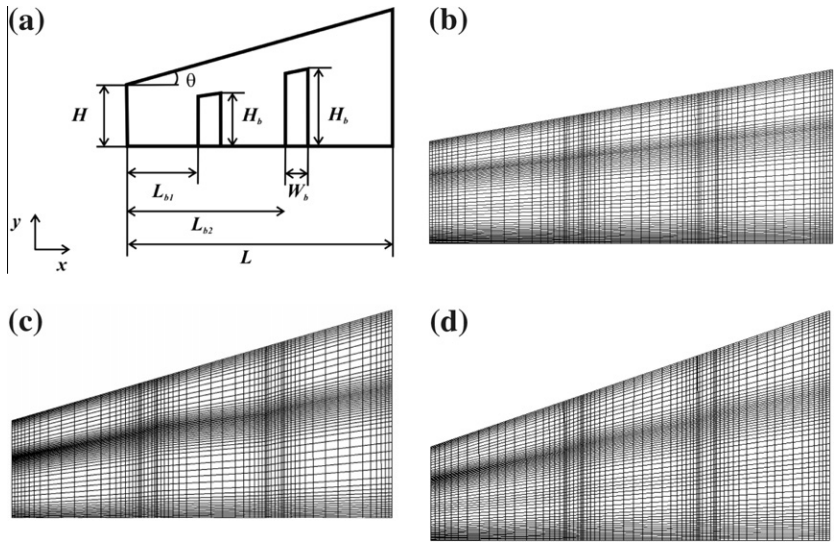

Fig. 1. General schematic configurations for $H_b = 2H^*/3$. (a) Physical model, (b) $\theta = 10°$, (c) $\theta = 15°$, and (d) $\theta = 20°$.

momentum equation. We approximate this term using the Boussinesq approximation. The flow field is considered to be steady-state, laminar, and two-dimensional. Therefore, the governing equations for the fluid flow and heat transfer are those expressing the conservation of mass, momentum, and energy. In dimensional form, the transport equations are given by:

$$\frac{\partial u}{\partial x} + \frac{\partial v}{\partial y} = 0, \tag{1}$$

$$\frac{\partial(uu)}{\partial x} + \frac{\partial(vu)}{\partial y} = -\frac{1}{\rho}\frac{\partial p}{\partial x} + \frac{\partial}{\partial x}\left(\nu\frac{\partial u}{\partial x}\right) + \frac{\partial}{\partial y}\left(\nu\frac{\partial u}{\partial y}\right), \tag{2}$$

$$\frac{\partial(uv)}{\partial x} + \frac{\partial(vv)}{\partial y} = -\frac{1}{\rho}\frac{\partial p}{\partial y} + \frac{\partial}{\partial x}\left(\nu\frac{\partial v}{\partial x}\right) + \frac{\partial}{\partial y}\left(\nu\frac{\partial v}{\partial y}\right) + g\beta(T - T_C), \tag{3}$$

$$\frac{\partial(uT)}{\partial x} + \frac{\partial(vT)}{\partial y} = \alpha\left(\frac{\partial^2 T}{\partial x} + \frac{\partial^2 T}{\partial y}\right), \tag{4}$$

where u (m/s) is the velocity in x-direction, v (m/s) is the velocity in y-direction, ρ (kg/m^3) is fluid density, ν (m^2/s) is kinematic viscosity, α (m^2/s) is thermal diffusivity ($\alpha = k/\rho c_p$), β (1/K) is the thermal expansion coefficient of air, T_C (K) is the cold (and reference) temperature, T (K) is temperature, and g (m/s^2) is gravitational acceleration.

Along the vertical wall, the following Dirichlet conditions are used:

$$T(x = 0, y) = T_H \tag{5}$$

$$T(x = L, y) = T_C \tag{6}$$

As shown in Eqs. (7)–(10), we assume no-slip velocities on all the walls:

$$u(x = 0, y) = v(x = 0, y) = 0, \tag{7}$$

$$u(x = L, y) = v(x = L, y) = 0 \tag{8}$$

$$u(x, y = 0) = v(x, y = 0) = 0 \tag{9}$$

$$u(x, y = H + x * tg(\theta)) = v(x, y = H + x * tg(\theta)) = 0. \tag{10}$$

The bottom and top surfaces remain insulated.

$$\left.\frac{\partial T}{\partial y}\right)_{y=0} = 0, \tag{11}$$

$$\left.\frac{\partial T}{\partial y}\right)_{y=H+x*tg(\theta)} = 0 \tag{12}$$

The energy balance at the baffle-fluid interface can be stated as:

$$-\frac{1}{Pr}(\hat{n}.\vec{\nabla}\theta_b)_i = -\frac{k_r}{Pr}(n.\vec{\nabla}\theta_b)_i \tag{13}$$

where $\hat{n}$ is a unit vector normal to the baffle-fluid interface, the subscript i refers to the interface, and k_r is the ratio between the thermal conductivity of the baffle and the convective fluid. The Ra number, for all results shown, is based on the shortest length of the vertical wall. Therefore, the Ra number is defined by

$$R = g\beta(T_H - T_C)H^3/\nu\alpha. \tag{14}$$

3. Numerical methodology

We solve the governing equations using the commercial computational fluid dynamics code ANSYS CFX version 12.0 [24]. In this code, the conservation equations for mass and momentum are solved together using the EbFVM. The resulting discrete system of linear equations is solved using an algebraic multigrid methodology called the additive correction multigrid method. The solution was considered converged when the sum of absolute normalized residuals for all cells in the domain solution was less than 10^{-12}, and double precision for all variables was used.

4. Results and discussion

This section is divided into four parts and presents the results for several cavity configurations, Ra and Pr numbers, and upper surface angles. Presented first is the mesh refinement study, then the results of streamlines and isotherms. Lastly, the results of local and average Nusselt numbers for all configurations are presented and discussed.

4.1. Mesh refinement study

A mesh refinement was performed for all cavities, investigating both Pr and Ra numbers. The analyses were based on the local and

the average Nusselt numbers along the hot and cold vertical walls, which were defined by

$$Nu_y = -\partial T/\partial x)_{x=0,x=L}/(T_H - T_C) \tag{15}$$

$$\overline{Nu} = \frac{1}{H*}\int_0^L Nu_y dy \cdots, \tag{16}$$

where H^* denotes the height of either the hot or cold wall. Based on this definition, the average Nusselt number along both the hot and cold walls must be the same.

The refinement was mainly focused at the walls of the trapezoidal cavity and next to the baffles, where the gradients were expected to be higher. Four different non-uniform grids composed of 31 × 34, 62 × 68, 124 × 136, and 248 × 272 volumes were used (Table 1). Table 1 presents the average Nusselt numbers obtained for each grid for baffle's height ($H_b = 2H^*/3$, and H^*), tilt angle of the upper surface equal to 15°, and Prandtl numbers (0.7, 10, and 130). Since the differences between the results obtained with grids formed by 62 × 68, 124 × 136, and 248 × 272 volumes were minor, (see Table 1) we chose the 62 × 68 non-uniform grid for all the simulations presented in this work. Fig. 1b–d shows the grid configurations used for the three investigated upper surface inclinations.

4.2. Flow structure and isotherms

Numerical simulations were performed for $Pr = 0.7$, 10, and 130, Ra numbers in the range of $10^3 \leqslant Ra \leqslant 10^6$, and three top surface inclination angles ($\theta = 10°$, 15°, and 20°) (see Fig. 1). The fluid motion and heating patterns are studied for heated vertical left walls, cooled vertical right walls, and adiabatic top and horizontal surfaces. The results for these configurations are presented in Figs. 2–8.

The isotherms and streamlines for all the investigated angles for $Pr = 0.7$, $H_b = H^*/3$, and $Ra = 10^3$ and 10^6, are respectively presented in Figs. 2 and 3. As expected, the flow is composed of single internal cells between the baffles and vertical walls. For $\theta = 15°$ and 20°, two vortices exist: one close to the hot wall and the other between the two baffles and the cold wall. These two vortices merged when the Rayleigh number was increased. We can see in Fig. 2 that for low Ra numbers, the temperature varies almost linearly inside the cavity, indicating that the conduction is a dominant heat transfer mode. Although the temperature gradient close to the vertical walls increases smoothly with the top surface inclination angle, the temperature profiles, in most of the cavity, present the same pattern for all inclination angles investigated. For small Ra numbers, three internal vortices exist in the cavity for all angles of the upper surface. However, when the Ra number was increased, the three internal vortices merged into a single cell for all inclination angles investigated (see Fig. 3). We can also see in Fig. 3 that the isotherms became more distorted and the convection became a dominant mode of heat transfer when the Ra number was increased. For the highest Ra number, a thermal stratification close to the lower and upper surfaces of the cavity is observed.

Figs. 4 and 5 illustrate the isotherms and streamlines for $Pr = 0.7$, $H_b = 2H^*/3$, and the three investigated angles, for $Ra = 10^3$ and 10^6, respectively. For small Ra numbers, similar isotherms to the ones presented in Fig. 2 were obtained and the three well-defined vortices already discussed formed inside the cavity. For large Ra numbers, a more stratified temperature field was observed and secondary vortices in the region between the baffles, and also close to the cold and hot walls, appeared. Figs. 4 and 5 reveal a similar pattern of isotherms and streamlines to those already presented in Figs. 2 and 3. The main difference is that the resistance to flow and heat transfer was amplified by the baffles dividing the cavity into almost three sub-cavities. The increase in resistance decreased the temperature and velocity gradients.

Fig. 6 and 7 show the isotherms and streamlines for Ra numbers, $Ra = 10^3$ and 10^6, respectively, and $H_b = H^*$. Once again, for small Ra numbers, the isotherms presented the same pattern already shown for $H_b = H^*/3$ and $2H^*/3$ for all inclination angles investigated. On the other hand, at higher Ra numbers, the thermal stratification also increased when the baffle height was increased. Consequently, the pattern of streamlines and isotherms differed, at larger Ra numbers and at higher baffle heights, from those for smaller Ra numbers and lower baffle heights. Furthermore, an increase in the thermal stratification might have still reduced the heat transfer inside the cavity. The flow was composed of multiple internal cells placed between the baffles and vertical walls. It is important to note that for the smallest Ra numbers, main vortices are formed while secondary vortices appear as the Ra number increases, Moreover, the number of secondary vortices increases with the inclination angle of the upper surface.

In order to see the effect of the Pr numbers in the fluid and heat transfer, the isotherms and streamlines for $\theta = 20°$, $Ra = 10^6$ and $H_b = 2H^*/3$ are shown in Fig. 8. Despite the difference in the order of magnitude between the chosen Pr numbers, we can see from Fig. 8 that the impact of the Pr number is much smaller than the other evaluated parameters. However, some differences in the streamline and isothermal pattern could be observed when the Pr number was changed from 0.7 to 10. The increase in the Pr number represents an increase in the momentum diffusivity in relation to thermal diffusivity; in that the higher Pr number, the more difficult the formation of secondary eddies and the less stratified the regions are.

4.3. Heat transfer rates: Local Nusselt numbers

This section presents the local Nusselt numbers along the cold and hot walls (Nu_c, Nu_h) for $10^3 \leqslant Ra \leqslant 10^6$, $Pr = 0.7$, $\theta = 10°$, 15° and 20° and $H_b = H^*/3$, $2H^*/3$ and H^*. This data helps to quantify the effect of the baffles' height, the Ra number, and tilt angle of the upper surface into the natural convection inside the cavity. In these figures, Y^* denotes the dimensionless height of the cold or hot wall.

Figs. 9–11 present the local Nusselt numbers along the hot wall (Nu_h) and cold wall (Nu_c) for three baffle heights: $H_b = H^*/3$, $2H^*/3$, and H^*, respectively, for $Ra = 10^3$ and 10^4. As Figs. 2, 4 and 6 present, the isotherms for $Ra = 10^3$, which are almost parallel to the vertical walls for all investigated tilt angles. This is due to less intensity of fluid circulation inside the cavity. Because of that the thermal gradient in Figs. 9–11 is almost zero along both vertical walls for all tilt angles and baffle heights. Furthermore, the conduction mode prevails in the cavity for small Ra numbers.

It is important to mention that the thermal gradient increases when both the Ra number and the upper wall's tilt angle increases, and it decreases when the baffle height increases. We can also see for all cases illustrated in Figs. 9–11 that the high values of local Nusselt numbers are found close to the lower section of the hot wall and close to the upper section of the cold wall. Also, for each Ra value, the highest value of the local Nusselt number is attained in the cold wall. We explain this by pointing out that the highest

Table 1
Average Nusselt number for different grids.

Mesh	$H_b = 2H^*/3$, $\theta = 15°$			$H_b = H^*$, $\theta = 20°$		
	Pr = 0.7	Pr = 10	Pr = 130	Pr = 0.7	Pr = 10	Pr = 130
31 × 34	7.6982	8.1204	8.1959	2.4421	2.1666	2.6832
62 × 68	7.0313	7.7592	7.8090	2.2335	2.6560	2.6775
124 × 136	7.0263	7.7489	7.9081	2.2324	2.6151	2.5614
248 × 272	7.0576	7.7732	7.9082	2.2320	2.6209	2.6071

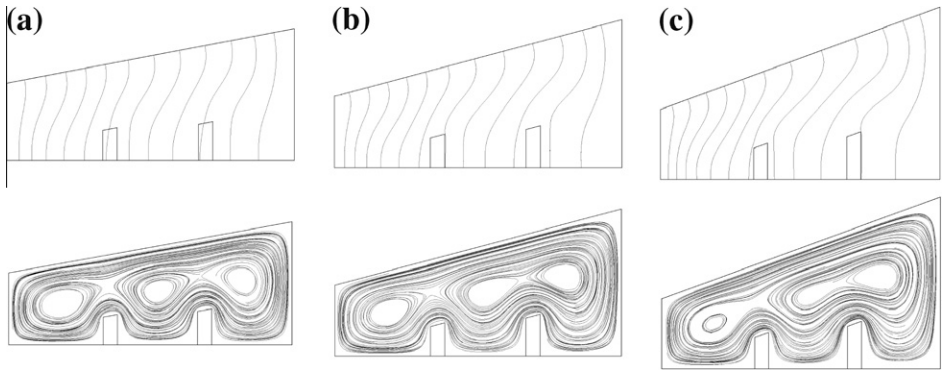

Fig. 2. Isotherms and streamlines for $Pr = 0.7$, $Ra = 10^3$, and $H_b = H^*/3$. (a) $\theta = 10°$, (b) $\theta = 15°$, and (c) $\theta = 20°$.

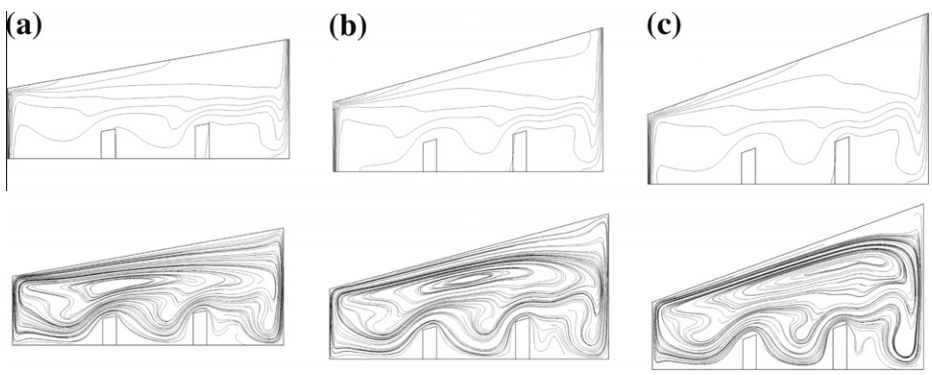

Fig. 3. Isotherms and streamlines for $Pr = 0.7$, $Ra = 10^6$, and $H_b = H^*/3$. (a) $\theta = 10°$, (b) $\theta = 15°$, and (c) $\theta = 20°$.

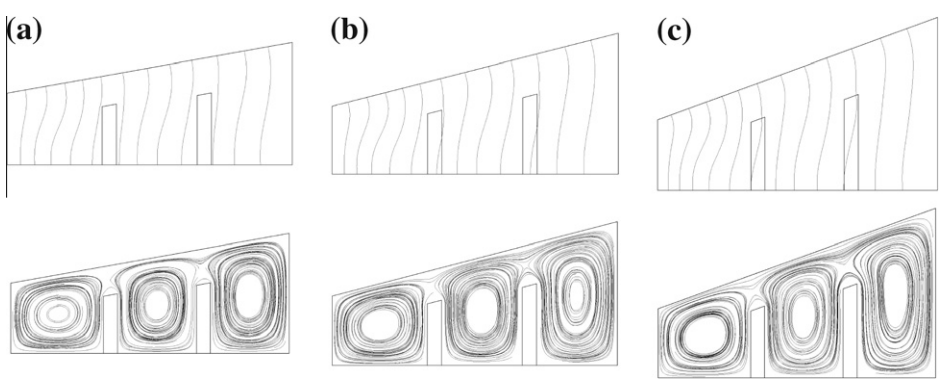

Fig. 4. Isotherms and streamlines for $Pr = 0.7$, $Ra = 10^3$, and $H_b = 2H^*/3$. (a) $\theta = 10°$, (b) $\theta = 15°$, and (c) $\theta = 20°$.

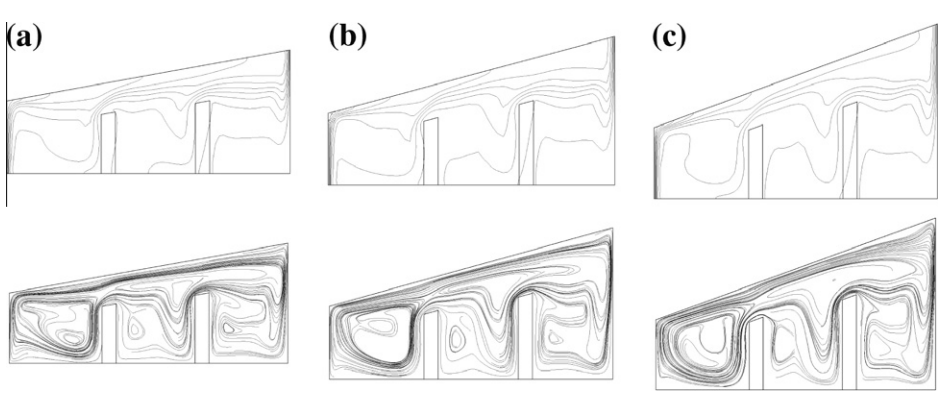

Fig. 5. Isotherms and streamlines for $Pr = 0.7$, $Ra = 10^6$, and $H_b = 2H^*/3$. (a) $\theta = 10°$, (b) $\theta = 15°$, and (c) $\theta = 20°$.

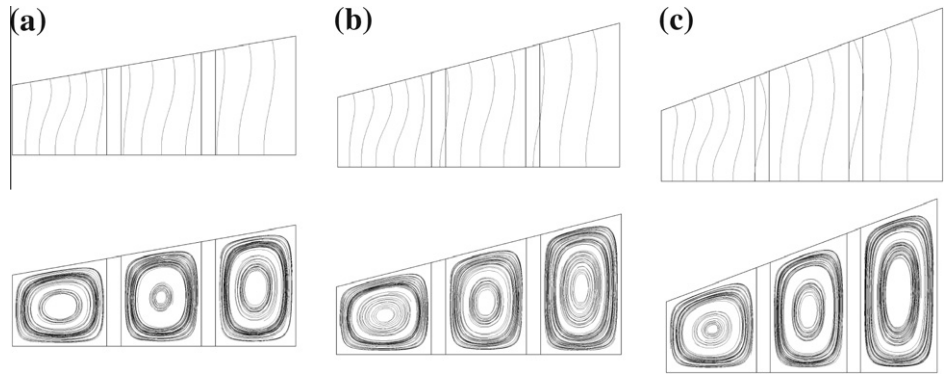

Fig. 6. Isotherms and streamlines for $Pr = 0.7$, $Ra = 10^3$, and $H_b = H^*$. (a) $\theta = 10°$, (b) $\theta = 15°$, and (c) $\theta = 20°$.

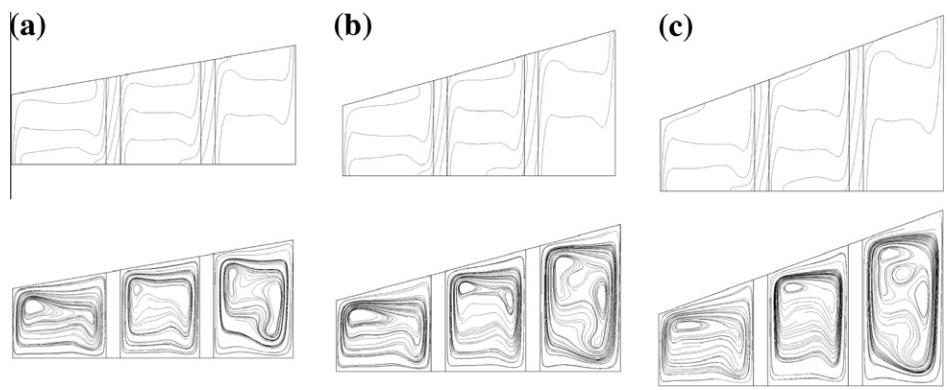

Fig. 7. Isotherms and streamlines for $Pr = 0.7$, $Ra = 10^6$, and $H_b = H^*$. (a) $\theta = 10°$, (b) $\theta = 15°$, and (c) $\theta = = 20°$.

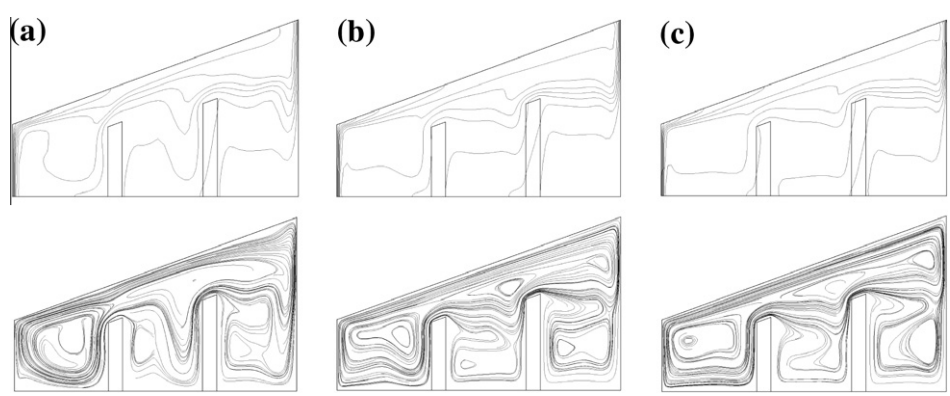

Fig. 8. Isotherms and streamlines for $\theta = 20°$, $Ra = 10^6$, and $H_b = 2H^*/3$. (a) $Pr = 0.7$, (b) $Pr = 10$, and (c) $Pr = 130$.

thermal stratification occurs in the lower section of the cold wall. This means that there is less space for the fluid coming from the upper inclined surface of the cavity to exchange energy with the cold vertical wall of the cavity. The temperature gradients will be smaller between the fluid going from the lower cold wall to the lower hot wall compared to the fluid going from the upper hot wall to the upper cold wall. Note that as the height of the baffle increased, the heat transfer drastically decreased.

Figs. 12–14 show the local Nusselt numbers at the hot and cold walls for three baffle heights, $H^*/3$, $2H^*/3$, and H^*, respectively, for $Ra = 10^5$ and 10^6, and three tilt angles, $\theta = 10°$, $15°$, and $20°$. The most significant findings here are the same as those presented for smaller Ra numbers above. More relevantly, for each investigated configuration, the local Nusselt values are greater than those obtained with Ra numbers 10^3 and 10^4, for all tilt angles investigated. It is worthwhile to mention that due to a higher intensity of circulation, convection starts to play a dominant role, then isotherms are gradually pushed toward the side walls for all tilt angles as shown in Figs. 3, 5 and 7 for $Ra = 10^6$. It is also observed that the zone of thermal stratification or thermal gradient is largest for $\theta = 20°$ for $Ra = 10^6$ and $H_b = H^*/3$. It is interesting to observe that due to enhanced circulation (baffle height $H_b = H^*/3$), isotherms are largely compressed near the vertical walls in the lower hot wall and upper cold wall, for $Ra = 10^6$ for all tilt angles (see Fig. 3). Fig. 12 shows that the magnitude of Nu_c and Nu_h is greater at these regions for all investigated tilt angles. When the baffles height increases (see Figs. 13 and 14), the fluid has less space to exchange energy along the vertical walls of the cavity; thus, heat transfer is decreased. When the baffle height was equal to H^*, the conduction mode nearly dominates the heat transfer.

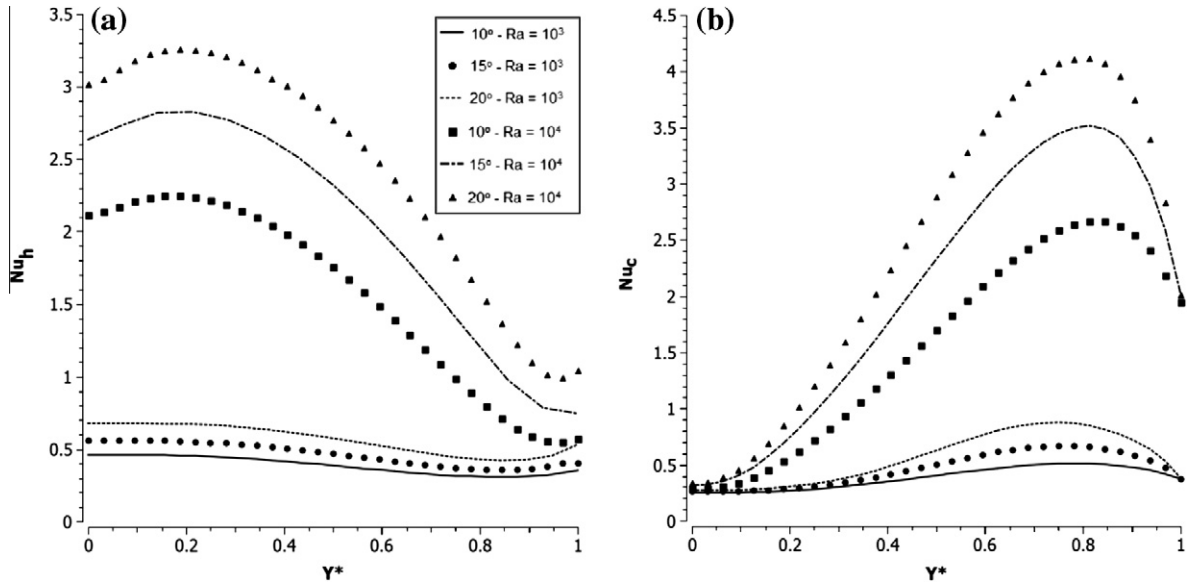

Fig. 9. Local Nusselt number for $Ra = 10^3$ and 10^4, $Pr = 0.7$, $\theta = 10°$, 15° and 20°, $H_b = H^*/3$. (a) Hot and (b) cold wall.

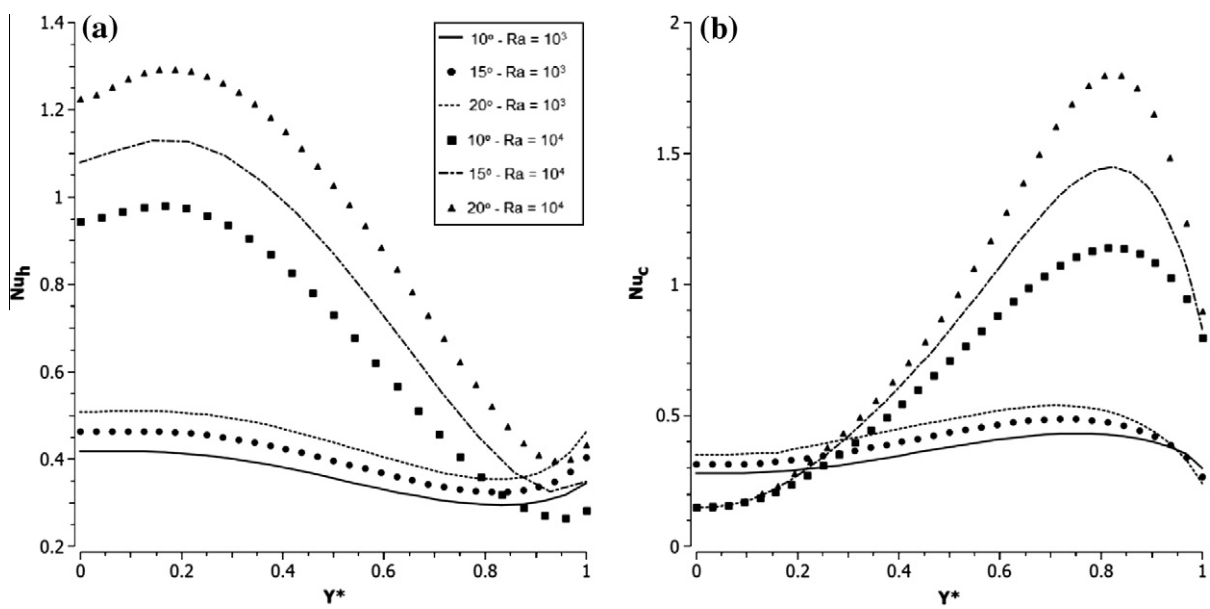

Fig. 10. Local Nusselt number for $Ra = 10^3$ and 10^4, $Pr = 0.7$, $\theta = 10°$, 15° and 20°, $H_b = 2H^*/3$. (a) Hot and (b) cold wall.

Moukalled and Darwish [10] reported the same behavior for trapezoidal cavities with one baffle when the height of the baffle was increased from $H^*/3$ to $2H^*/3$.

4.4. Heat transfer rates: Average Nusselt numbers

The overall effects upon the heat transfer rates are displayed in this section where the average Nusselt number values for cavity with the left vertical wall heated and the right vertical wall cooled are described in Tables 2–4 for $Pr = 0.7$, 10, and 130, respectively. The average Nusselt number is obtained using Eqs. (15) and (16). The average Nusselt number was investigated in this paper for three inclination angles of the upper surface (10°, 15°, and 20°), for the wide range of Ra numbers, $10^3 \leqslant Ra \leqslant 10^6$, and baffle heights ($H^*/3$, $2H^*/3$, and H^*). As previously discussed, it is possible to observe from Table 1 that for a fixed Ra number, a significant reduction in heat transfer occurs when the baffle height is increased, mainly for the largest Ra numbers.

For the smallest Ra number, the average Nusselt number tends to be a constant value when the baffle height is increased. For a given baffle height, the total heat transfer increases with increasing Ra values, due to an increase in convection heat transfer. In addition, the average Nusselt increases smoothly with increasing the tilt angle, due to the increase in the temperature gradient close to the hot and cold walls. As expected, the average Nusselt number increases when the Pr number is increased, due to a decrease in the thermal boundary-layer thickness along the walls. However, such an effect is limited to a specific Pr number. We can observe that the average Nusselt numbers for $Pr = 10$ and 130 for each investigated configuration are very close to each other. This result agrees with the results found by Moukalled and Darwish [13] for other configurations.

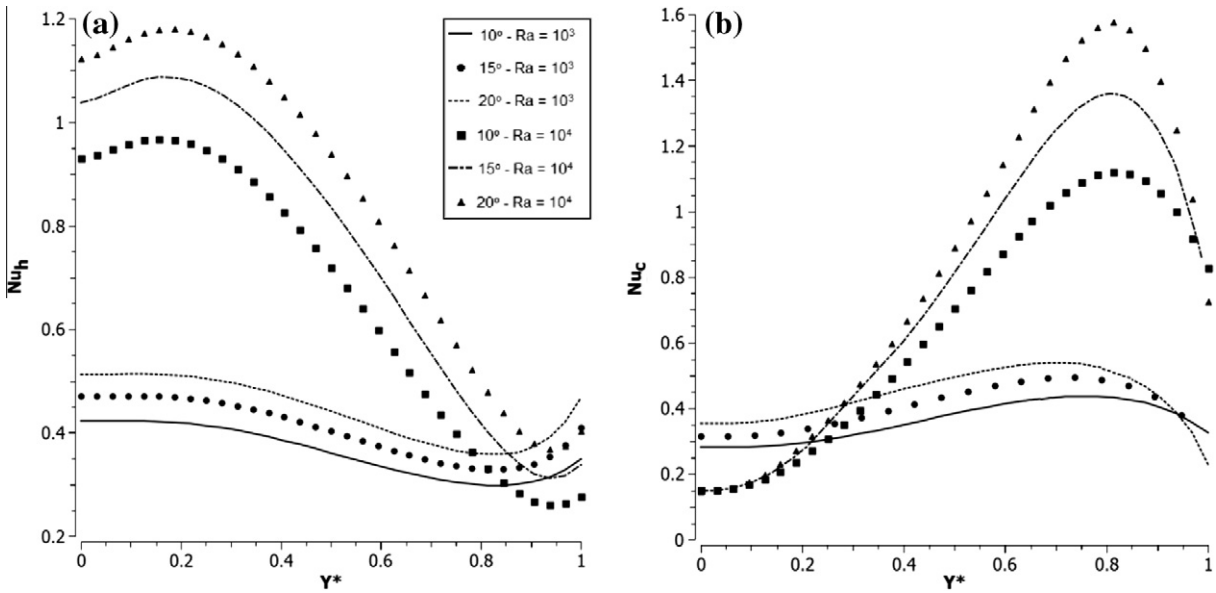

Fig. 11. Local Nusselt number for $Ra = 10^3$ and 10^4, $Pr = 0.7$, $\theta = 10°$, 15° and 20°, $H_b = H^*$. (a) Hot and (b) cold wall.

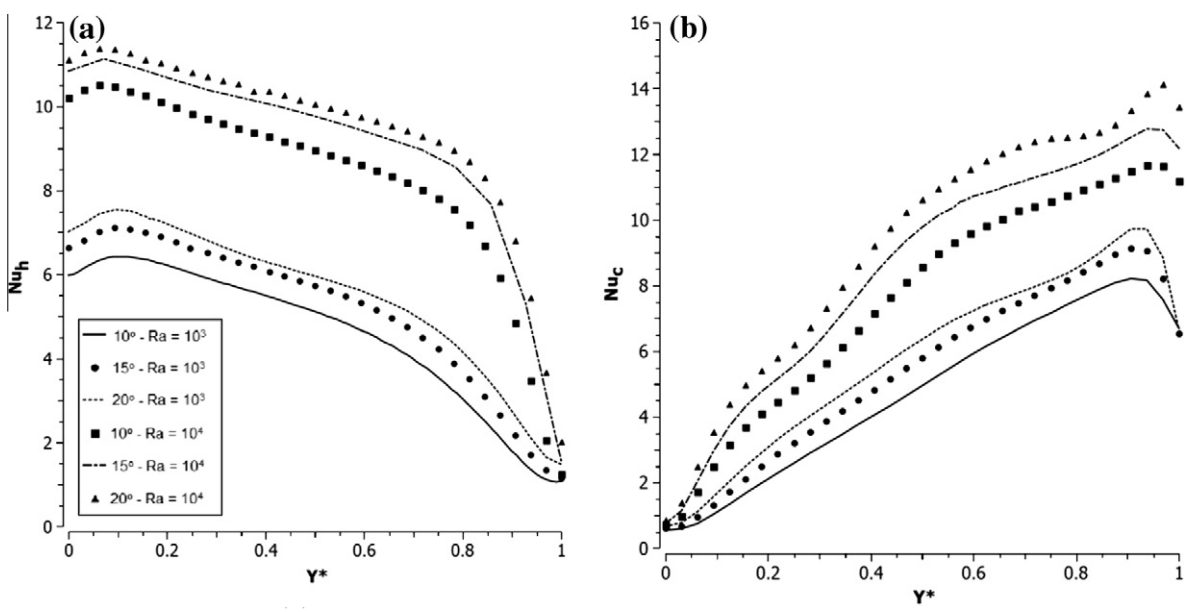

Fig. 12. Local Nusselt number for $Ra = 10^5$ and 10^6, $Pr = 0.7$, $\theta = 10°$, 15° and 20°, $H_b = H^*/3$. (a) Hot and (b) cold wall.

In order to combine all the average Nusselt numbers, three correlation equations are proposed for each baffle height investigated. Eqs. (17)–(19) present the average Nusselt number for $H_b = H^*$, $2H^*/3$ and $H^*/3$, respectively. In these equations, the correction factor used by Peters et al. [25] and Marcondes et al. [26] is included. The use of such a factor is justified by Bejan [27], who showed that $Nu \sim (RaPr)^n$ for low Pr numbers, and $Nu \sim (Ra)^n$ for high Pr numbers, where n is a constant, and $\sim$ means the same order of magnitude. The mean relative error of the simulation data set and each one of the correlations were the following: 6.0% for Eq. (17), 14.9% for Eq. (18), and 17.3% for Eq. (19). Deviations between numerical and predicted average Nusselt numbers by correlation were calculated using the multiple correlation coefficient (Pearson coefficient, R^2) whose results were 0.984, 0.973, and 0.945 for Eqs. (17)–(19), respectively.

$$\overline{Nu} = 0.06505(F \times RaH_{\max})^{0.22708} \tag{17}$$

$$\overline{Nu} = 0.00890(F \times RaH_{\max})^{0.43211} \tag{18}$$

$$\overline{Nu} = 0.08463(F \times RaH_{\max})^{0.30106} \tag{19}$$

where $Ra_{H_{\max}} = \frac{g\beta(T_H - T_C)H_{\max}^3}{\nu\alpha}$, $H_{\max} = H + Ltg(\theta)$, and $F = \frac{\Pr}{1+\Pr}$.

The average Nusselt number for all configurations, Pr and Ra numbers, and tilt angles of the upper surface, are presented in Fig. 15 as well as in Eqs. (17)–(19) for each baffle height. Although, there are some discrepancies between the proposed correlation and the obtained results, the results are nearly well-adjusted for every baffle height investigated.

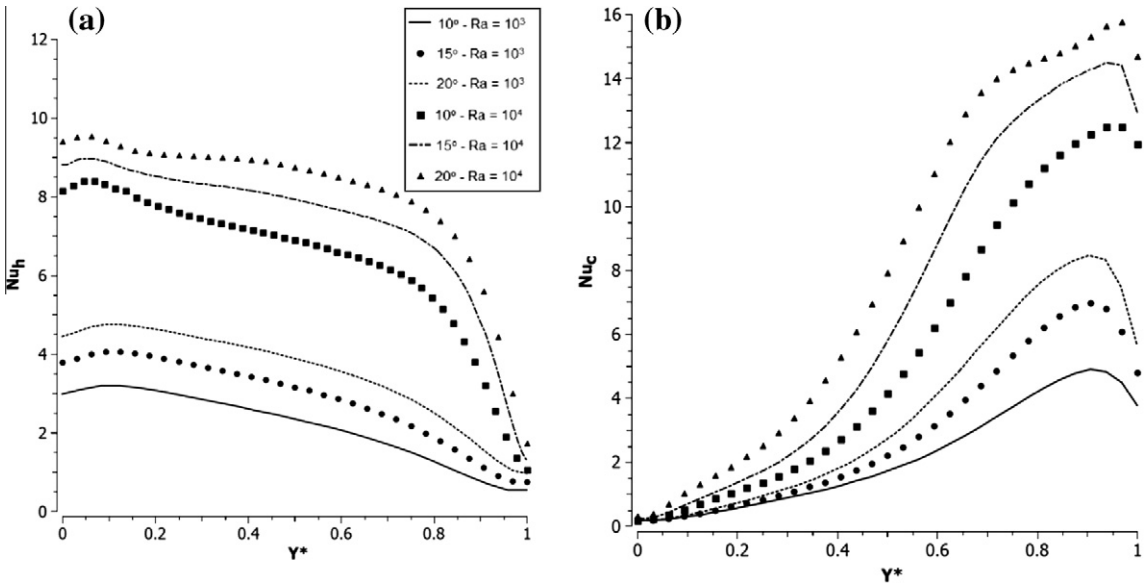

Fig. 13. Local Nusselt number for $Ra = 10^5$ and 10^6, $Pr = 0.7$, $\theta = 10°$, 15° and 20°, $H_b = 2H^*/3$. (a) Hot and (b) cold wall.

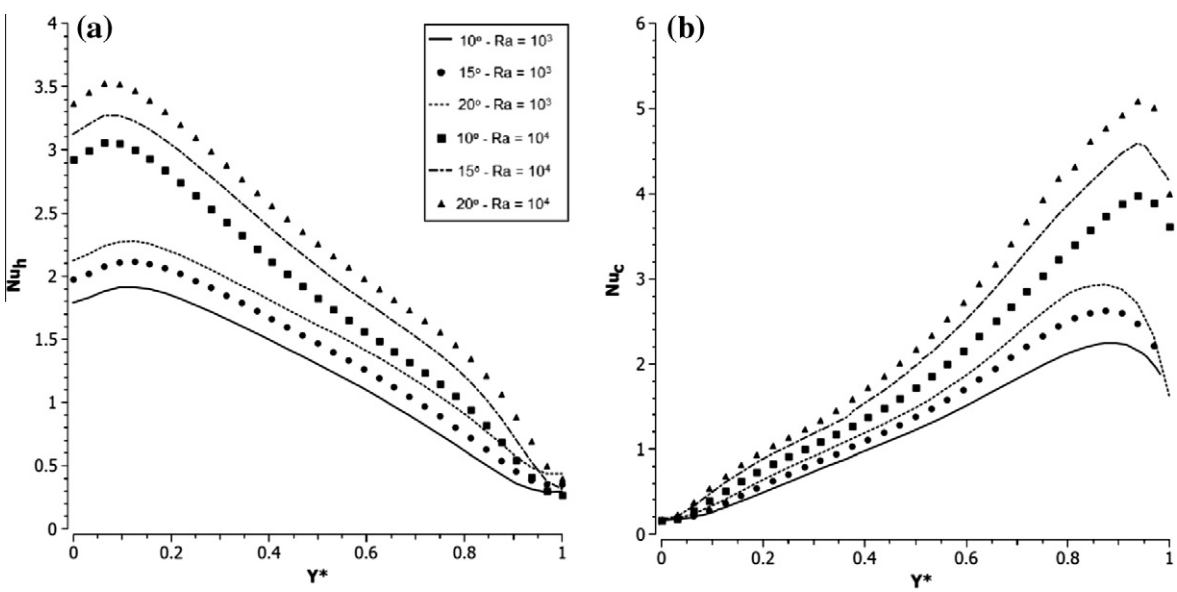

Fig. 14. Local Nusselt number for $Ra = 10^5$ and 10^6, $Pr = 0.7$, $\theta = 10°$, 15° and 20°, $H_b = H^*$. (a) Hot and (b) cold wall.

Table 2
Average Nusselt numbers ($\overline{Nu}$) along the cold right and hot left walls for $Pr = 0.7$.

θ	H*/3	10°			15°			20°	
Ra		2H*/3	H*	H*/3	2H*/3	H*	H*/3	2H*/3	H*
10^3	0.385848	0.357316	0.362609	0.445600	0.399500	0.404890	0.565453	0.440343	0.444634
10^4	1.564760	0.674230	0.663574	1.976000	0.782600	0.751900	2.456350	0.930542	0.851829
10^5	4.573560	2.149980	1.225690	5.265000	2.762300	1.350100	5.649540	3.547060	1.531030
10^6	8.175380	6.292120	1.876910	8.241300	7.031300	2.028800	8.958220	8.107960	2.233493

5. Conclusions

The present paper investigated the effect of two offset baffles in natural convection within trapezoidal enclosures, where the left short vertical wall was heated and the right long vertical wall was cooled, and the upper inclined surface and lower horizontal surface were kept adiabatic. The governing equations were solved through the EbFVM, using the commercial simulator CFX. Several physical parameters were investigated such as *Ra* and *Pr* numbers and geometric parameters such as the baffles' height and the inclination of the upper surface of the cavity. The results were presented in terms of isotherms, streamlines, as well as local and average Nusselt numbers. Three correlation equations for the average Nusselt number for each baffle's height were also presented.

Table 3
Average Nusselt numbers ($\overline{Nu}$) along the cold right and hot left walls for $Pr = 10$.

θ	$H^*/3$	10°			15°			20°	
Ra		$2H^*/3$	H^*	$H^*/3$	$2H^*/3$	H^*	$H^*/3$	$2H^*/3$	H^*
10^3	0.38621	0.35762	0.36267	0.45310	0.40001	0.40560	0.57844	0.44039	0.44473
10^4	1.59825	0.67958	0.66793	2.13850	0.80380	0.76460	2.60565	0.95998	0.86040
10^5	5.64858	2.39577	1.25716	6.32020	3.33760	1.40870	6.89481	4.22403	1.57649
10^6	9.13593	7.73247	2.18514	9.95270	8.74890	2.42070	10.66040	9.52453	2.65594

Table 4
Average Nusselt numbers ($\overline{Nu}$) along the cold right and hot left walls for $Pr = 130$.

θ	$H^*/3$	10°			15°			20°	
Ra		$2H^*/3$	H^*	$H^*/3$	$2H^*/3$	H^*	$H^*/3$	$2H^*/3$	H^*
10^3	0.37855	0.37950	0.36250	0.45280	0.40030	0.40560	0.57584	0.44657	0.44438
10^4	1.59983	0.71943	0.66680	2.13880	0.84040	0.76460	2.60563	0.98969	0.86017
10^5	5.65417	2.39936	1.26379	6.31990	3.34810	1.40920	6.88673	4.23640	1.57359
10^6	9.16527	7.80047	2.18038	9.95420	8.90810	2.42210	10.66835	9.68453	2.67749

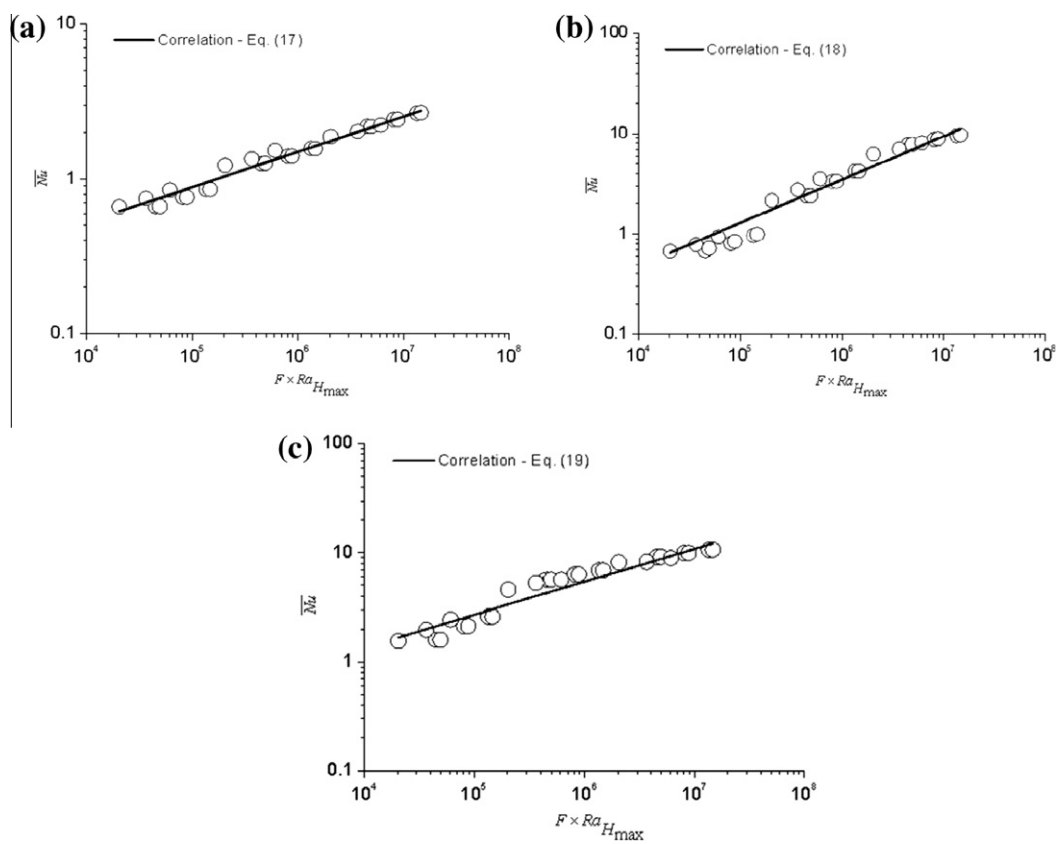

Fig. 15. Average Nusselt number for (a) H^*, (b) $2H^*/3$, and (c) $H^*/3$.

Numerical results showed that when *Ra* is fixed, a significant reduction in heat transfer occurs when the baffle height was increased. On the other hand, it was observed that for a given baffle height, the total heat transfer increased substantially with increasing *Ra* numbers, while the average Nusselt increased smoothly with an increasing tilt angle.

Acknowledgments

The authors would like to thank CNPq (The National Council for Scientific and Technological Development of Brazil) and the ANP (National Petroleum Agency) for their financial support through the following processes: 568221/2008-7, 302786/2008-2/PQ, 306231/2009-3/PQ, 504102/2009-5/PQ, 475689/2010-0, and ANP (PRH 09).

References

[1] L. Iyican, Y. Bayazitoglu, L.C. Witte, An analytical study of natural convective heat transfer within trapezoidal enclosure, J. Heat Transfer 102 (8) (1980) 640–647.
[2] L. Iyican, L.C. Witte, Y. Bayazitoglu, An experimental study of natural convection in trapezoidal enclosures, J. Heat Transfer 102 (8) (1980) 648–653.
[3] S.W. Lam, R. Gani, J.G. Simons, Experimental and numerical studies of natural convection in trapezoidal cavities, J. Heat Transfer 111 (2) (1989) 372–377.
[4] T.S. Lee, Numerical experiments with fluid convection in tilted nonrectangular enclosures, Numer. Heat Transfer, Part. A 19 (4) (1991) 487–499.

[5] M. Peric, Natural convection in trapezoidal cavities, Numer. Heat Transfer, Part A 24 (2) (1993) 213–219.
[6] R.A. Kuyper, C.J. Hoogendoorn, Laminar natural convection flow in trapezoidal enclosures, Numer. Heat Transfer, Part A 28 (1) (1995) 55–67.
[7] F. Moukalled, S. Acharya, Buoyancy-induced heat transfer in partially divided trapezoidal cavities, Numer. Heat Transfer, Part A 32 (8) (1997) 787–810.
[8] F. Moukalled, S. Acharya, Natural convection in trapezoidal cavities with baffles mounted on the upper inclined surfaces, Numer. Heat Transfer, Part. A 37 (6) (2000) 545–565.
[9] F. Moukalled, S. Acharya, Natural convection in trapezoidal cavities with two offset baffles, AIAA J. Thermophysics and Heat Transfer 15 (2) (2001) 212–218.
[10] F. Moukalled, M. Darwish, Natural convection in a partitioned trapezoidal cavity heated from the side, Numer. Heat Transfer, Part. A 43 (5) (2003) 543–563.
[11] M. Boussaid, A. Djerrada, M. Bouhadef, Thermosolutal transfer within trapezoidal cavity, Numer. Heat Transfer, Part. A 43 (5) (2003) 431–448.
[12] F. Moukalled, M. Darwish, Natural convection in a trapezoidal enclosure heated from the side with a baffle mounted on its upper inclined surface, Heat Transfer Eng. 25 (8) (2004) 80–93.
[13] F. Moukalled, M. Darwish, Buoyancy induced heat transfer in a trapezoidal enclosure with offset baffles, Numer. Heat Transfer, Part. A 52 (4) (2007) 337–355.
[14] E. Natarajan, S. Roy, T. Basak, Effect of various thermal boundary conditions on natural convection in a trapezoidal cavity with linearly heated side wall(s), Numer. Heat Transfer, Part. B 52 (6) (2007) 551–568.
[15] E. Natarajan, T. Basak, S. Roy, Natural convection flows in a trapezoidal enclosure with uniform and non-uniform heating of bottom wall, Int. J. Heat Mass Transfer 51 (3–4) (2008) 747–756.
[16] T. Basak, S. Roy, A. Singh, B.D. Pandey, Natural convection flow simulation for various angles in a trapezoidal enclosure with linearly heated side wall(s), Int. J. Heat Mass Transfer 52 (19–20) (2009) 4413–4425.
[17] T. Basak, S. Roy, I. Pop, Heat flow analysis for natural convection within trapezoidal enclosures based on heatline concept, Int. J. Heat Mass Transfer 52 (11–12) (2009) 2471–2483.
[18] K. Lasfer, M. Bouzaiane, T. Lili, Numerical study of laminar natural convection in a side-heated trapezoidal cavity at various inclined heated sidewalls, Heat Transfer Eng. 31 (5) (2010) 362–373.
[19] E. Fontana, A. da Silva, V.C. Mariani, F. Marcondes, The influence of baffles on the natural convection in trapezoidal cavities, Numer. Heat Transfer, Part. A 58 (2) (2010) 125–145.
[20] I. Tmartnhad, M. El Alami, M. Najam, A. Oubarra, Numerical investigation on mixed convection flow in a trapezoidal cavity heated from below, Energy Conv. Manage 49 (11) (2008) 3205–3210.
[21] E. Papanicolaou, V. Belessiotis, Double-diffusive natural convection in an asymmetric trapezoidal enclosure: unsteady behavior in the laminar and the turbulent-flow regime, Int. J. Heat Mass Transfer 48 (1) (2005) 191–209.
[22] S.B. Paramane, A. Sharma, Consistent implementation and comparison of FOU, CD, SOU, and QUICK Convection Schemes on Square, Skew, Trapezoidal, and Triangular Lid-Driven Cavity Flow, Numer. Heat Transfer, Part. B 54 (1) (2008) 84–102.
[23] R. Roslan, H. Saleh, I. Hashim, Buoyancy-driven heat transfer in nanofluid-filled trapezoidal enclosure with variable thermal conductivity and viscosity, Numer. Heat Transfer, Part. A 60 (10) (2011) 867–882.
[24] User guides for ANSYS CFX Release 12.0, ANSYS Europe Ltd.
[25] S. Peters, F. Marcondes, A.T. Prata, Numerical solution for natural convection between vertical and inclined asymmetrically heated parallel plates, J, Bra. Soc. Mech. Sci. 15 (1993) 368–375.
[26] F. Marcondes, V.S. Melo, J.M. Gurgel, Numerical analysis of natural convection in parallel, convergent, and divergent open-ended channels, Int. J. Numer. Methods Heat Fluid Flow 16 (3) (2006) 304–323.
[27] A. Bejan, Convection Heat Transfer, second ed., Wiley, New York, 1995.